Atmospheric
Chemistry
and Physics

NO$_2$-initiated multiphase oxidation of SO$_2$ by O$_2$ on CaCO$_3$ particles

Ting Yu[1,*], Defeng Zhao[1,a,*], Xiaojuan Song[1], and Tong Zhu[1]

[1]BIC-ESAT and SKL-ESPC, College of Environmental Sciences and Engineering, Peking University,
Beijing, 100871, China
[a]now at: Department of Atmospheric and Oceanic Sciences & Institute of Atmospheric Sciences,
Fudan University, Shanghai, 200438, China
[*]These authors contributed equally to this work.

Correspondence: Tong Zhu (tzhu@pku.edu.cn)

Abstract. The reaction of SO$_2$ with NO$_2$ on the surface of aerosol particles has been suggested to be important in sulfate formation during severe air pollution episodes in China. However, we found that the direct oxidation of SO$_2$ by NO$_2$ was slow and might not be the main reason for sulfate formation in ambient air. In this study, we investigated the multiphase reaction of SO$_2$ with an O$_2$ / NO$_2$ mixture on single CaCO$_3$ particles using Micro-Raman spectroscopy. The reaction converted the CaCO$_3$ particle to a Ca(NO$_3$)$_2$ droplet, with CaSO$_4 \cdot$2H$_2$O solid particles embedded in it, which constituted a significant fraction of the droplet volume at the end of the reaction. The reactive uptake coefficient of SO$_2$ for sulfate formation was on the order of 10^{-5}, which was higher than that for the multiphase reaction of SO$_2$ directly with NO$_2$ by 2–3 orders of magnitude. According to our observations and the literature, we found that in the multiphase reaction of SO$_2$ with the O$_2$ / NO$_2$ mixture, O$_2$ was the main oxidant of SO$_2$ and was necessary for radical chain propagation. NO$_2$ acted as the initiator of radical formation, but not as the main oxidant. The synergy of NO$_2$ and O$_2$ resulted in much faster sulfate formation than the sum of the reaction rates with NO$_2$ and with O$_2$ alone. We estimated that the multiphase oxidation of SO$_2$ by O$_2$ initiated by NO$_2$ could be an important source of sulfate and a sink of SO$_2$, based on the calculated lifetime of SO$_2$ regarding the loss through the multiphase reaction versus the loss through the gas-phase reaction with OH radicals. Parameterization of the reactive uptake coefficient of the reaction observed in our laboratory for further model simulation is needed, as well as an integrated assessment based on field observations, laboratory study results, and model simulations to evaluate the importance of the reaction in ambient air during severe air pollution episodes, especially in China.
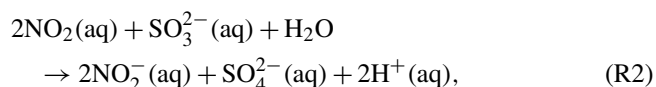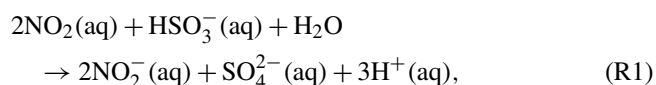
1 Introduction

It has been suggested that multiphase or heterogeneous oxidation of SO$_2$ potentially plays an important role in sulfate formation in the atmosphere (Seinfeld and Pandis, 2006). During the severe pollution episodes that occur frequently in China, high sulfate concentrations cannot be explained by the gas-phase oxidation of SO$_2$ and its well known aqueous chemistry (Zheng et al., 2015a; Cheng et al., 2016), highlighting the role of underappreciated heterogeneous oxidation or multiphase pathways.
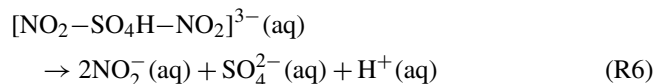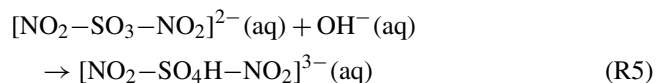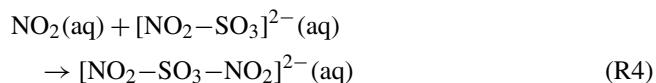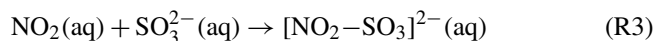
Recently, the multiphase oxidation of SO$_2$ by NO$_2$ has been introduced in air quality model simulations to explain the discrepancy between the modeled and observed sulfate concentration during severe pollution episodes in China (Cheng et al., 2016; Gao et al., 2016; Wang et al., 2016; Xue et al., 2016), despite the uncertainties in the kinetic parameters for SO$_2$ oxidation and in the pH value of aerosol particles in China (Wang et al., 2016; Cheng et al., 2016; Liu et al., 2017; Guo et al., 2017). However, according to our recently published results (Zhao et al., 2018), the direct oxidation of SO$_2$ by NO$_2$ could not contribute significantly to sulfate formation in the atmosphere because the reactive uptake coefficient of SO$_2$ for sulfate formation due to direct oxidation by NO$_2$ is very low ($\sim 10^{-8}$).

Although the contribution of the direct oxidation of SO$_2$ by NO$_2$ to sulfate formation is not significant, NO$_2$ may be involved in other oxidation pathways of SO$_2$. It has been reported that the reaction of NO$_2$ with SO$_3^{2-}$ and HSO$_3^-$ in the bulk aqueous phase can form the SO$_3^{\bullet-}$ radical, which can further react with O$_2$ and produce a series of radicals that oxidize S(IV) species (Littlejohn et al., 1993). The reaction pathway may result in a fast SO$_2$ oxidation due to the potential synergy of NO$_2$ and O$_2$.
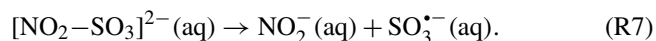
Despite such a reaction mechanism for SO$_2$ oxidation being proposed, its role in SO$_2$ oxidation in the ambient atmosphere is not well established. Most previous studies have focused on the direct reaction of SO$_2$ with NO$_2$, including the determination of its rate constant (Lee and Schwartz, 1983; Clifton et al., 1988; Shen and Rochelle, 1998; Spindler et al., 2003; Nash, 1979; Huie and Neta, 1986). According to the reaction products and their reported yields (Lee and Schwartz, 1983; Clifton et al., 1988), the overall reaction equations of the direct reaction of SO$_2$ with NO$_2$ are as follows:

$$2NO_2(aq) + HSO_3^-(aq) + H_2O$$
$$\rightarrow 2NO_2^-(aq) + SO_4^{2-}(aq) + 3H^+(aq), \tag{R1}$$
$$2NO_2(aq) + SO_3^{2-}(aq) + H_2O$$
$$\rightarrow 2NO_2^-(aq) + SO_4^{2-}(aq) + 2H^+(aq), \tag{R2}$$

and the reactions are proposed to proceed via NO$_2$–S(IV) adduct complexes (Clifton et al., 1988).

$$NO_2(aq) + SO_3^{2-}(aq) \rightarrow [NO_2-SO_3]^{2-}(aq) \tag{R3}$$
$$NO_2(aq) + [NO_2-SO_3]^{2-}(aq)$$
$$\rightarrow [NO_2-SO_3-NO_2]^{2-}(aq) \tag{R4}$$
$$[NO_2-SO_3-NO_2]^{2-}(aq) + OH^-(aq)$$
$$\rightarrow [NO_2-SO_4H-NO_2]^{3-}(aq) \tag{R5}$$
$$[NO_2-SO_4H-NO_2]^{3-}(aq)$$
$$\rightarrow 2NO_2^-(aq) + SO_4^{2-}(aq) + H^+(aq) \tag{R6}$$

Additionally, NO$_2$–S(IV) adduct complexes may decompose as follows (Spindler et al., 2003):

$$[NO_2-SO_3]^{2-}(aq) \rightarrow NO_2^-(aq) + SO_3^{\bullet-}(aq). \tag{R7}$$

However, studies of the oxidation rate of SO$_2$ at the O$_2$ concentrations relevant to the ambient atmosphere and the potential influence of the synergy of NO$_2$ and O$_2$ on the oxidation rate are very limited (Turšič et al., 2001; He et al., 2014), except for a few studies which investigated SO$_2$ oxidation in the presence of NO$_2$ as well as O$_2$ (Littlejohn et al., 1993; Shen and Rochelle, 1998; Santachiara et al., 1990). Moreover, previous studies have mainly focused on the reaction in bulk solution and only few studies have investigated the oxidation of SO$_2$ by NO$_2$ on aerosol particles (Santachiara et al.,

1990, 1993). On aerosol particles, water activity, pH, ionic strength, the presence of other compounds or ions, and the role of the particle surface are different from dilute bulk solution and may affect the reaction process and reaction rate. Therefore, further studies of the multiphase reaction of SO$_2$ with O$_2$ / NO$_2$ mixtures on aerosol particles are required to determine the kinetic parameters and the mechanism of the reaction.

In this study, we investigated the multiphase reaction of SO$_2$ with O$_2$ in the presence of NO$_2$ on CaCO$_3$ particles. We quantified the reactive uptake coefficient of SO$_2$ due to the reaction with an O$_2$ / NO$_2$ / H$_2$O mixture. Based on our observations and the existing literature, we further discussed the reaction mechanism. Furthermore, we estimated the role of the multiphase oxidation of SO$_2$ by O$_2$ in the presence of NO$_2$ in the atmosphere.

2 Experimental

The experiments were conducted using a flow reaction system and the setup is shown in Fig. S1 in the Supplement. The experimental setup and procedure used have been described in detail in previous studies (Zhao et al., 2018, 2011; Liu et al., 2008). A gas mixture of NO$_2$, SO$_2$, O$_2$, N$_2$, and water vapor reacted with particles deposited on a substrate in the flow reaction cell. The concentrations of SO$_2$ and NO$_2$ were controlled using mass flow controllers by varying the flow rates of SO$_2$ (2000 ppm in high purity N$_2$, National Institute of Metrology P.R. China), NO$_2$ (1000 ppm in high purity N$_2$, Messer, Germany), and synthetic air (20 % O$_2$ (high purity grade: 99.999 %, Beijing Haikeyuanchang Practical Gas Co., Ltd.) and 80 % N$_2$ (high purity grade: 99.999 %, Beijing Haikeyuanchang Practical Gas Co., Ltd.)). Relative humidity (RH) was controlled by regulating the flow rates of reactant gases, dry synthetic air, and humidified synthetic air. Humidified synthetic air was prepared by bubbling synthetic air through fritted glass in water. In some experiments, the O$_2$ concentrations were varied by regulating the mixing ratios of O$_2$ and N$_2$ to investigate the effect of O$_2$. SO$_2$ / O$_2$ / NO$_2$ / H$_2$O mixtures flowed through the reaction cell and reacted with individual stationary CaCO$_3$ particles, which were deposited on a Teflon$^{\circledR}$ FEP film substrate annealed to a silicon wafer. RH and temperature were measured using a hygrometer (HMT100, Vaisala, Vantaa, Finland) at the exit of the reaction cell. Additionally, temperature was measured using another small temperature sensor (Pt 100, 1/3 DIN B, Heraeus, Hanau, Germany) in the reaction cell. All the experiments were conducted at 298 ± 0.5 K. The experiments were conducted under two RHs (72 and 82 %) at 75 ppm SO$_2$ and 75 ppm NO$_2$.

During the reaction, particles were monitored in situ via a glass window on the top of the reaction cell using a Micro-Raman spectrometer (LabRam HR800, HORIBA Jobin Yvon, Kyoto, Japan) to obtain microscopic images

and Raman spectra. A 514 nm excitation laser was used, and back-scattering Raman signals were detected. The details of the instrument are described elsewhere (Liu et al., 2008; Zhao et al., 2011). Because the particles were larger than the laser spot in this study ($\sim 1.5\,\mu$m), confocal Raman mapping was used to measure the spectra at different locations on a particle to obtain the chemical information of the entire particle. The mapping area was rectangular and was slightly larger than the particle, with mapping steps of $1 \times 1\,\mu$m. Raman spectra in the range of 800–3900 cm^{-1} were acquired with an exposure time of 1 s for each mapping point. Raman spectra were analyzed using Labspec 5 software (HORIBA Jobin Yvon). Raman peaks were fitted to Gaussian–Lorentzian functions to obtain peak positions and peak areas at different locations on the particle. The peak areas were then added together to obtain the peak area for the entire particle.

Particles of CaCO₃ (98 %, Sigma-Aldrich, USA), with average diameters of about 7–10 μm, as specified by the supplier, were used in the experiments. The CaCO₃ particles were rhombohedron crystals; X-ray diffraction analysis indicated that they were calcite (Fig. S2). Individual particles were prepared by dripping a dilute CaCO₃ suspended solution onto Teflon® FEP film using a pipette and then drying the sample in an oven at 80 °C for 10 h.

The amount of CaSO₄ as a reaction product was quantified based on Raman peak areas and particle sizes. The details of the method are described in our previous study (Zhao et al., 2018). Briefly, the amount of reaction product CaSO₄ formed was determined as a function of time using Raman peak areas. Raman peak areas were converted to the amount of compound formed using a calibration curve obtained from pure CaSO₄ particles of different sizes, which were determined according to microscopic images. The reaction rate, i.e., the sulfate production rate, was derived from the amount of sulfate formed as a function of time. The reactive uptake coefficient of SO₂ for sulfate formation (γ) was further determined from the reaction rate and collision rate of SO₂ on the surface of a single particle.

$$\gamma = \frac{\frac{d\{SO_4^{2-}\}}{dt}}{Z} \qquad (1)$$

$$Z = \frac{1}{4}cA_s[SO_2] \qquad (2)$$

$$c = \sqrt{\frac{8RT}{\pi M_{SO_2}}}, \qquad (3)$$

where R is the gas constant, T is temperature, M_{SO_2} is the molecular weight of SO₂, c is the mean molecular velocity of SO₂, A_s is the surface area of an individual particle, and Z is the collision rate of SO₂ on the surface of a particle. $\{SO_4^{2-}\}$ indicates the amount of sulfate in the particle phase in moles. The average reaction rate and surface area of particles during the multiphase reaction period were used to derive the reac-

tive uptake coefficient. The period was chosen to start after the induction period when ~ 10 % of the final sulfate was formed. [SO₂] indicates the concentration of SO₂ in the gas phase.

The influence of gas-phase diffusion on reactive uptake was evaluated using the resistor model described by Davidovits et al. (2006) and references therein, as well as using the gas-phase diffusion correction factor for a reactive uptake coefficient according to the method described by Pöschl et al. (2007). The reactive uptake of SO₂ was found to not be limited by gas-phase diffusion (see details in the Supplement, Sect. S1).
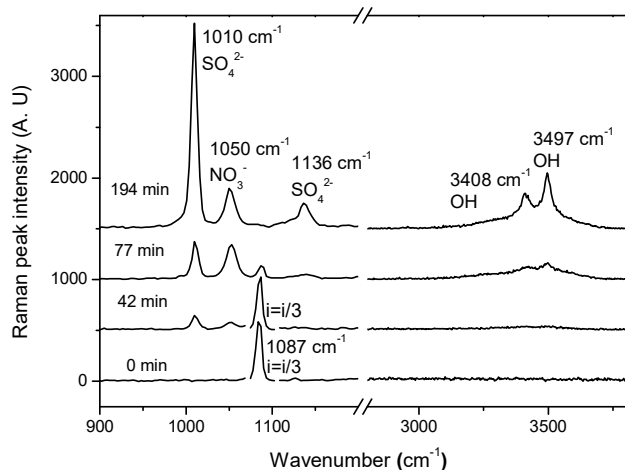
In addition, we conducted experiments of the reaction SO₂ with only O₂ on both CaCO₃ solid particles and internally mixed CaCO₃ / Ca(NO₃)₂ particles (with CaCO₃ embedded in Ca(NO₃)₂ droplets), while keeping other conditions the same as the reaction of SO₂ with an O₂ / NO₂ mixture. These experiments of the multiphase oxidation of SO₂ by O₂ can help determine the role of NO₂ in the reaction of SO₂ with an O₂ / NO₂ mixture.

3 Results and discussion

3.1 Reaction products and changes in particle morphology

Figure 1 shows the Raman spectra of a CaCO₃ particle during the multiphase reaction of SO₂ with O₂ / NO₂ / H₂O on its surface. The peak at 1087 cm^{-1} was assigned to the symmetric stretching of carbonate ($\nu_s(CO_3^{2-})$) (Nakamoto, 1997). During the reaction, the peak at 1087 cm^{-1} decreased continuously and finally disappeared as new peaks were observed. The peak at 1050 cm^{-1} was assigned to the symmetric stretching of nitrate ($\nu_s(NO_3^-)$). The peaks at 1010 and 1136 cm^{-1} were assigned to the symmetric stretching ($\nu_s(SO_4^{2-})$) and asymmetric stretching ($\nu_{as}(SO_4^{2-})$) of sulfate in gypsum (CaSO₄ · 2H₂O), respectively (Sarma et al., 1998). In addition, after the reaction, a broad envelope in the range of 2800–3800 cm^{-1} assigned to the stretching of the OH bond in water molecules was observed. Above this envelope, there were two peaks at 3408 and 3497 cm^{-1}, which were assigned to OH bond stretching in crystallization water of CaSO₄ · 2H₂O (Sarma et al., 1998; Ma et al., 2013).

During the multiphase reaction with the SO₂ / O₂ / NO₂ / H₂O mixture, the CaCO₃ particles displayed a remarkable change in morphology. The original CaCO₃ particle was a rhombohedron crystal (Fig. 2i.a). As the reaction proceeded, its edges became smoother and later a transparent droplet layer formed, which had a newly formed solid phase embedded in it (Fig. 2i.d). The size of the new solid phase grew during the reaction (Fig. 2i.d–f) and it seemed to contain many micro-crystals. Raman mapping revealed that the new solid phase consisted of CaSO₄ · 2H₂O

Figure 1. Raman spectra of a CaCO$_3$ particle during the multiphase reaction of SO$_2$ with O$_2$ / NO$_2$ / H$_2$O on the particle. SO$_2$: 75 ppm, NO$_2$: 75 ppm, RH: 72 %, O$_2$: 20 %. The peak intensity of carbonate (1087 cm^{-1}) at 0 and 42 min was divided by 3 for clarity.

(Fig. 2iv), and the surrounding aqueous layer consisted of Ca(NO$_3$)$_2$ (Fig. 2iii).

The particle morphology change shown in Fig. 2 was significantly different from the morphology change in the direct reaction of SO$_2$ with NO$_2$ (Zhao et al., 2018), where the CaCO$_3$ particle was first converted to a spherical Ca(NO$_3$)$_2$ droplet and then needle-shaped CaSO$_4$ crystals formed inside the droplet (Zhao et al., 2018). Moreover, the amount of CaSO$_4$ formed in this study was much higher than that in the direct reaction of SO$_2$ with NO$_2$. The CaSO$_4$ solid particle constituted a significant fraction of the volume of the droplet, while in the direct reaction of SO$_2$ with NO$_2$ the few needle-shaped CaSO$_4$ crystals that formed only constituted a small fraction of the droplet volume (Zhao et al., 2018).

3.2 Reaction process

During the reaction, the amounts of carbonate, nitrate, and sulfate were determined as a function of time, as shown in Fig. 3. At the beginning of the reaction, the amount of carbonate decreased slowly, while the amount of nitrate and sulfate increased slowly. After a period of induction of around 50 min, the reaction accelerated significantly, leading to a rapid consumption of carbonate and production of nitrate and sulfate. The decrease in the amount of carbonate and the increase in the amount of nitrate was because carbonate reacted continuously with NO$_2$ and H$_2$O, forming Ca(NO$_3$)$_2$. The detailed mechanisms of the multiphase reaction of carbonate with NO$_2$ and H$_2$O were discussed in our previous studies (Li et al., 2010; Zhao et al., 2018). The mechanism of sulfate formation is discussed in detail in Sect. 3.4 of the present study. Finally, the carbonate was completely consumed, and the amounts of nitrate and sulfate leveled off.

Table 1. Reactive uptake coefficient of SO$_2$ for sulfate formation at 82 % RH and at different O$_2$ concentrations.
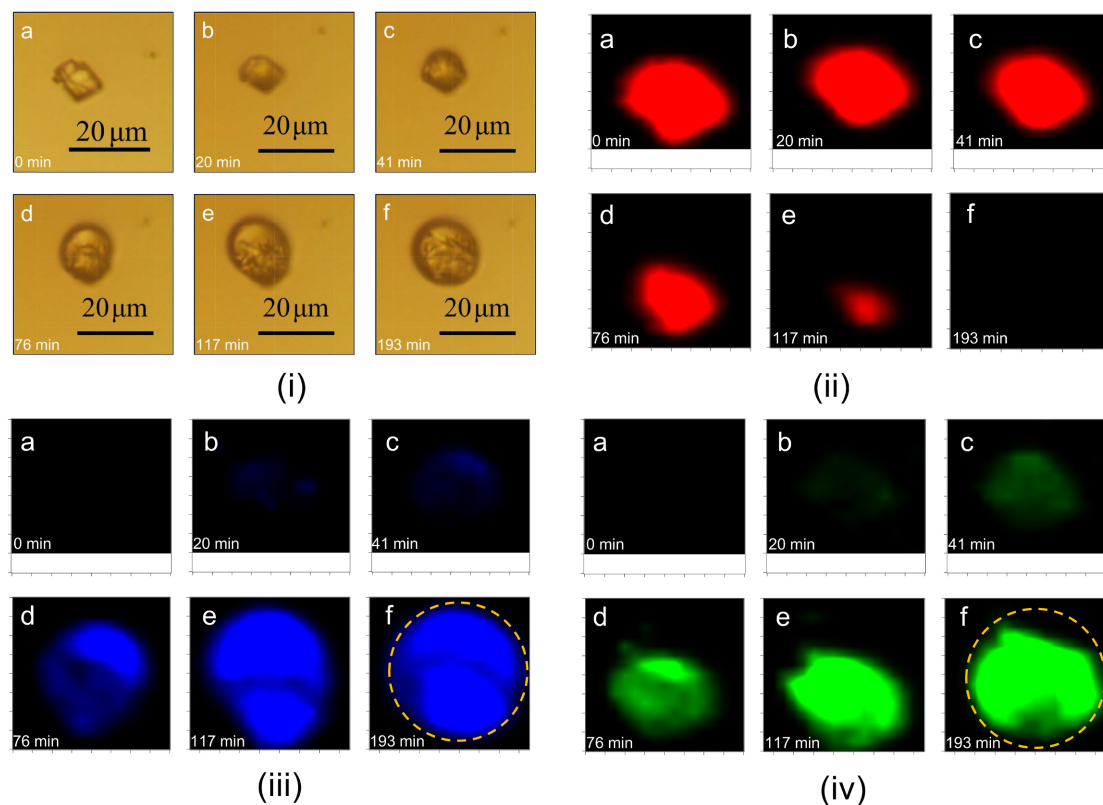
SO$_2$ / NO$_2$ / O$_2$ concentration	γ
75 ppm / 75 ppm / 86 %	1.7×10^{-5}
75 ppm / 75 ppm / 20 %	1.2×10^{-5}
75 ppm / 75 ppm / 5 %	3.5×10^{-6}

Figure 3 shows that nitrate and sulfate were formed simultaneously during the reaction. This contrasts with the observations made during the direct reaction of SO$_2$ with NO$_2$, where nitrate was formed first, and sulfate was essentially formed after the complete conversion of CaCO$_3$ particles to Ca(NO$_3$)$_2$ droplets (Zhao et al., 2018). Moreover, the time taken for carbonate to be completely consumed was longer in this study than in the direct reaction of SO$_2$ with NO$_2$ ($\sim$ 120 vs. $\sim$ 40 min) when other conditions were kept the same (Zhao et al., 2018).

3.3 Reactive uptake coefficient of SO$_2$

The reactive uptake coefficients of SO$_2$ for sulfate formation (γ) in the reaction of SO$_2$ with the O$_2$ / NO$_2$ / H$_2$O / N$_2$ mixture on CaCO$_3$ with various O$_2$ concentrations are shown in Table 1. The value of γ for the reaction of SO$_2$ with O$_2$ / NO$_2$ at three O$_2$ concentrations (5, 20, and 86 %) was in the range of $(0.35–1.7) \times 10^{-5}$, and was 1.2×10^{-5} in synthetic air. This latter value was 2–3 orders of magnitude higher than that for the reaction of SO$_2$ directly with NO$_2$ under similar conditions (Zhao et al., 2018). When other conditions were kept constant, γ increased with the O$_2$ concentration. This indicates that O$_2$ played a key role in enhancing the oxidation rate of SO$_2$.

The role of O$_2$ in enhancing the reactive uptake of SO$_2$ reported here is consistent with the findings in some previous studies. For example, the data of Littlejohn et al. (1993) showed that the sulfite oxidation rate increases with the O$_2$ concentration (0–5 % by volume). Shen and Rochelle (1998) also found that in the presence of O$_2$, the aqueous sulfite oxidation rate is enhanced. By investigating the oxidation of SO$_2$ by NO$_2$ in monodispersed water droplets growing on carbon nuclei, Santachiara et al. (1990) found that the sulfate formation rate with 2 % O$_2$ is much higher than that without O$_2$. However, our findings, as well as those in the studies referred to above, are in contrast to those reported by Lee and Schwartz (1983), who found that changing from N$_2$ to air as a carrier gas only increases the bisulfite oxidation rate by no more than 10 %. The difference between our study and Lee and Schwartz (1983) could be due to the difference in O$_2$ diffusion from the gas to the condensed phase and the different mechanisms between the multiphase reaction on particles and the aqueous reaction.

Figure 2. Microscopic image **(i)** and Raman mapping image of carbonate **(ii)**, nitrate **(iii)**, and sulfate **(iv)** on the CaCO$_3$ particle during the multiphase reaction SO$_2$ with O$_2$ / NO$_2$ / H$_2$O on the particle. Panels **(a–f)** correspond to the reaction times of 0, 20, 41, 76, 117, and 193 min. SO$_2$: 75 ppm, NO$_2$: 75 ppm, RH: 72 %, O$_2$: 20 %. The mapping images of carbonate, nitrate, and sulfate are made using the peak area at 1050, 1010, and 1087 cm^{-1}, respectively. The red, blue, and green colors indicate the peak intensity of carbonate, nitrate, and sulfate, respectively. The dashed lines in panel **(iii.f)** and **(iv.f)** indicate the shape of the droplet at the end of the reaction.

Only few studies have reported the S(IV) oxidation rate in the reaction of S(IV) with O$_2$ / NO$_2$ mixtures (Turšič et al., 2001; Littlejohn et al., 1993). However, due to the limiting step by the aqueous-phase mass transfer, it is difficult to quantitatively compare the reaction rates in those studies with the uptake coefficient in our study and the rate constants determined by Lee and Schwartz (1983) and Clifton et al. (1988). For example, a rate constant of 2.4×10^3 mol^{-1} L s^{-1} (at pH 3) can be derived from the results of Turšič et al. (2001), which is much lower than the values reported by Lee and Schwartz (1983) and Clifton et al. (1988). This can be attributed to the limiting step by the aqueous-phase mass transfer because the characteristic mixing time in the aqueous phase in Turšič et al. (2001) was likely much longer than that of Lee and Schwartz (1983) (1.7–5.3 s), according to the HSO$_3^-$ concentration time series reported by Turšič et al. (2001).
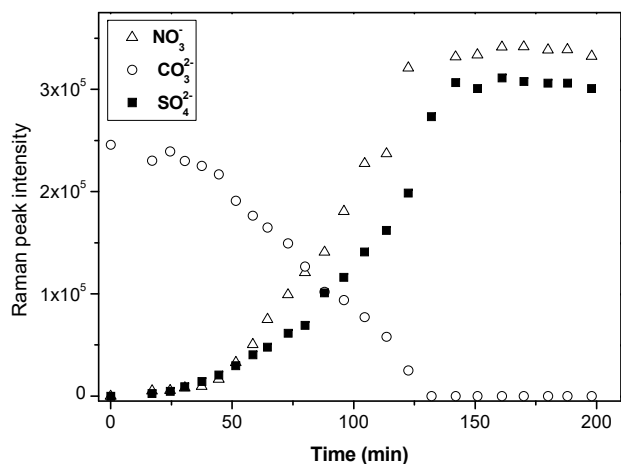
It is important to note that the concentrations of NO$_2$ and SO$_2$ used in this study are much higher than those in the ambient atmosphere. High concentrations of reactant gases are often used in laboratory studies in order to simulate the ambient reactions at the timescale of days or weeks and to obtain high signal-to-noise ratios for detecting products within minutes or hours. In the ambient atmosphere, the reactive uptake coefficient of SO$_2$ should be lower than that in this study due to the lower NO$_2$ concentrations when other conditions are comparable, and the chemical and physical processes observed in this study, such as changes in particle composition, phase, hygroscopicity, and pH, should be much slower due to the lower concentrations of NO$_2$ and SO$_2$.

3.4 Reaction mechanism

In the multiphase reaction of SO$_2$ with O$_2$ / NO$_2$ / H$_2$O on CaCO$_3$ particles, we found that CaCO$_3$ reacted with NO$_2$ and H$_2$O and produced Ca(NO$_3$)$_2$, which deliquesced, forming liquid water, and provided a site for the aqueous oxidation of SO$_2$. This process is similar to the direct reaction of SO$_2$ with NO$_2$ on CaCO$_3$ particles. The details of this part of the reaction mechanism were discussed in our previous study (Zhao et al., 2018).

Once the aqueous phase was formed, SO$_2$ could undergo multiphase reactions with O$_2$ / NO$_2$. The mechanism of the direct aqueous reaction of S(IV) with NO$_2$ in the absence of

Figure 3. Time series of the Raman peak intensity of NO_3^-, SO_4^{2-}, and CO_3^{2-} during the reaction of SO_2 with O_2 / NO_2 / H_2O on CaCO$_3$ particles. SO_2: 75 ppm, NO_2: 75 ppm, RH: 72 %, O_2: 20 %. The intensity of NO_3^-, SO_4^{2-}, and CO_3^{2-} show the peak area at 1050, 1010, and 1087 cm^{-1}, respectively, in Raman spectra obtained by Raman mapping.

O_2 is complex. Previous studies have proposed two different mechanisms for the reaction. One involves $SO_3^{\bullet-}$ radical formation (Littlejohn et al., 1993; Shen and Rochelle, 1998; Turšič et al., 2001) (referred to as the "free-radical chain" mechanism), while the other involves the formation of NO_2–S(IV) complexes (Clifton et al., 1988), but no radical formation (referred to as the "NO_2–S(IV) complex" mechanism).

According to the NO_2–S(IV) complex mechanism, the presence of O_2 should not affect the SO_2 oxidation rate; however, in this study, a substantial enhancement in the SO_2 oxidation rate was observed in the presence of O_2 compared with that in the absence of O_2. Therefore, the NO_2–S(IV) complex mechanism was less likely to have been important in this study.

In the free-radical chain mechanism, the $SO_3^{\bullet-}$ radical is proposed to be formed (Reaction R8, Table 2), which is based on the observation of $S_2O_6^{2-}$ formation, with $S_2O_6^{2-}$, known to be the combination reaction product of $SO_3^{\bullet-}$ (Eriksen, 1974; Hayon et al., 1972; Deister and Warneck, 1990; Brandt et al., 1994; Waygood and McElroy, 1992). In addition to SO_4^{2-} and NO_2^-, $S_2O_6^{2-}$ was detected with an appreciable yield using Raman spectroscopy, following the reaction of NO_2 with aqueous sulfite (Littlejohn et al., 1993). $S_2O_6^{2-}$ was also observed in the aqueous oxidation of bisulfite in an N_2-saturated solution in the presence of Fe(III) using ion interaction chromatography (Podkrajšek et al., 2002). The $SO_3^{\bullet-}$ radical can react via two pathways, forming either $S_2O_6^{2-}$ or SO_4^{2-} (Reactions R9–R11, Table 2). Reactions R9–R11 have been well established in studies of S(IV) oxidation by other pathways, including OH oxidation, photo-oxidation, and transition metal catalyzed oxidation (Eriksen,

1974; Hayon et al., 1972; Deister and Warneck, 1990; Brandt et al., 1994; Brandt and Vaneldik, 1995; Waygood and McElroy, 1992). In addition, although previous studies have not reported the direct observation of the $SO_3^{\bullet-}$ radical in the aqueous reaction of S(IV) with NO_2, $SO_3^{\bullet-}$ was observed in the reaction of NO_2^- with SO_3^{2-} in an acidic buffer solution (pH = 4.0) using electron spin resonance (Shi, 1994). Because NO_2^- is formed in the aqueous reaction of SO_2 with NO_2, and $S_2O_6^{2-}$ as the combination reaction product of $SO_3^{\bullet-}$ is observed (Littlejohn et al., 1993), $SO_3^{\bullet-}$ formation is plausible.

In the presence of O_2, the $SO_3^{\bullet-}$ radical can react rapidly with O_2, forming the $SO_5^{\bullet-}$ radical (Reaction R12, Table 2). Following this reaction, a number of chain reactions can occur to ultimately form sulfate (Littlejohn et al., 1993; Seinfeld and Pandis, 2006; Shen and Rochelle, 1998) (Reactions R13–R16, Table 2). Littlejohn et al. (1993) observed that the amount of $S_2O_6^{2-}$ relative to SO_4^{2-} formed in the aqueous reaction of NO_2 with sulfite decreases in the presence of O_2 compared with the reaction in the absence of O_2. At low NO_2 concentrations (< 5 ppm), $S_2O_6^{2-}$ is undetectable in the presence of O_2. This indicates that O_2 suppresses the reaction pathway of $S_2O_6^{2-}$ formation (Reaction R9, Table 2). Because the $SO_3^{\bullet-}$ radical can react rapidly with O_2, forming the $SO_5^{\bullet-}$ radical, and would therefore be consumed, the suppression of $S_2O_6^{2-}$ formation can be attributed to the reaction of $SO_3^{\bullet-}$ with O_2 (Reaction R12, Table 2). Reactions (R12)–(R16) have been well established by studies of the oxidation of S(IV) by OH or photo-oxidation, and all the radicals have been observed (Hayon et al., 1972; Huie et al., 1989; Huie and Neta, 1987; Chameides and Davis, 1982; Seinfeld and Pandis, 2006).

The free-radical chain mechanism is consistent with the findings of this study and is therefore more plausible. The enhancement of the SO_2 oxidation rate in the reaction of SO_2 with O_2 / NO_2 / H_2O on CaCO$_3$ particles compared with that in the direct reaction of SO_2 with NO_2 / H_2O was attributed to O_2. Although during the reaction in the absence of O_2 – i.e., the direct oxidation of SO_2 by NO_2 – the $SO_3^{\bullet-}$ radical can be formed (Reaction R7), the reaction chain cannot propagate (Reactions R12–R16). Therefore, the S(IV) oxidation rate and the reactive uptake coefficient of SO_2 were much lower than those in the presence of O_2. According to the difference between the reactive uptake coefficient in this study and in the direct reaction of SO_2 with NO_2 (Zhao et al., 2018), the sulfate production rate via chain reactions due to the presence of O_2 (20 %) was 2–3 orders of magnitude faster than the direct oxidation of SO_2 by NO_2. This indicates that sulfate production in the reaction of SO_2 with O_2 / NO_2 was largely due to O_2 oxidation via the chain reaction pathway, i.e., "autoxidation" of S(IV), rather than the direct oxidation of SO_2 by NO_2, and thus O_2 was the main oxidant of SO_2.

In addition to the two mechanisms above, Spindler et al. (2003) proposed a reaction mechanism involving first
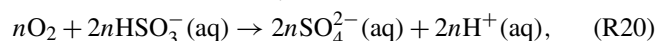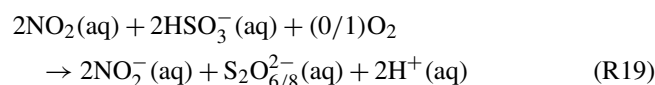
Table 2. Summary of the mechanism of the reaction S(IV) with O$_2$ / NO$_2$.

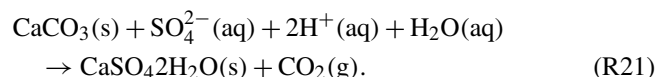| Step	Reactions	
Initiation	$NO_2(aq) + HSO_3^-(aq) \rightarrow NO_2^-(aq) + SO_3^{\bullet -}(aq) + H^+(aq)$	(R8)
Propagation	$SO_3^{\bullet -}(aq) + O_2(aq) \rightarrow SO_5^{\bullet -}(aq)$	(R12)
	$SO_5^{\bullet -}(aq) + HSO_3^-(aq) \rightarrow HSO_5^-(aq) + SO_3^{\bullet -}(aq)$	(R13)
	$HSO_5^-(aq) + HSO_3^-(aq) \rightarrow 2SO_4^{2-}(aq) + 2H^+(aq)$	(R14)
	$SO_5^{\bullet -}(aq) + HSO_3^-(aq) \rightarrow SO_4^{2-}(aq) + SO_4^{\bullet -}(aq) + H^+(aq)$	(R15)
	$SO_4^{\bullet -}(aq) + HSO_3^-(aq) \rightarrow SO_4^{2-}(aq) + SO_3^{\bullet -}(aq) + H^+(aq)$	(R16)
Termination	$SO_3^{\bullet -}(aq) + SO_3^{\bullet -}(aq) \rightarrow S_2O_6^{2-}(aq)$	(R9)
	$SO_3^{\bullet -}(aq) + SO_3^{\bullet -}(aq) \rightarrow SO_3^{2-}(aq) + SO_3$	(R10)
	$SO_3(aq) + H_2O \rightarrow SO_4^{2-}(aq) + 2H^+(aq)$	(R11)
	$SO_4^{\bullet -}(aq) + SO_4^{\bullet -}(aq) \rightarrow S_2O_8^{2-}(aq)$	(R17)
	$SO_5^{\bullet -}(aq) + SO_5^{\bullet -}(aq) \rightarrow S_2O_8^{2-}(aq) + O_2(aq)$	(R18)

NO$_2$–S(IV) complex formation and subsequent SO$_3^{\bullet -}$ radical formation (Reactions R3, R7). NO$_2$–S(IV) complexes may establish an equilibrium with SO$_3^{\bullet -}$ in contrast to the direct formation of SO$_3^{\bullet -}$ via the reaction of NO$_2$ with SO$_2$. Higher concentration of O$_2$ favors the conversion of SO$_3^{\bullet -}$ to SO$_5^{\bullet -}$ and thus can reduce the SO$_3^{\bullet -}$ concentration, shifting the equilibrium to the product side and promoting the overall S(IV) oxidation. O$_2$ can act in a similar way as in the free-radical chain mechanism. Admittedly, we cannot rule out the possibility of a NO$_2$–S(IV) complex formation. But such a mechanism can still be classified as the free-radical chain mechanism since the S(IV) oxidation still proceeds via the radical chain reactions. Although the direct oxidation of SO$_2$ by NO$_2$ only accounted for a very small fraction of sulfate formation, NO$_2$ played an important role in the SO$_2$ oxidation by initiating the chain reactions via the production of the SO$_3^{\bullet -}$ radical (Reaction R7). In the experiment without NO$_2$, but with other reaction conditions the same, we were unable to detect sulfate after 5 h of reaction. This indicates that O$_2$ by itself cannot initiate the chain reactions (although it favors chain propagation), and that the oxidation of SO$_2$ by O$_2$ was slow. The effect on the SO$_2$ oxidation rate when both NO$_2$ and O$_2$ were present was much higher than the sum of the effect of NO$_2$ and O$_2$. We refer to this effect as the synergy of NO$_2$ and O$_2$, which resulted in the fast oxidation of SO$_2$ to form sulfate in this study. This effect is similar to a "ternary" reaction found with the reaction of NO$_2$–particles–H$_2$O or SO$_2$–particles–O$_3$ (Zhu et al., 2011), where the reaction rate can be much faster than the sum of the reaction rates for the reaction of the second and third reactant with the first reactant. In addition to acting as the initiator of chain reactions, NO$_2$ also contributed to the formation of the aqueous phase through the reaction with CaCO$_3$, forming Ca(NO$_3$)$_2$ as discussed above, which provided a site for S(IV) oxidation.

Based on the discussion above, we summarize the reaction mechanism that occurred in this study in Table 2. The reactions are classified as chain initiation, chain propagation, and chain termination. The dominant S(IV) species depends on pH. Due to the fast dissociations of SO$_2 \cdot$H$_2$O and HSO$_3^-$, reactions consuming one of these S(IV) species will result in instantaneous re-establishment of the equilibria between them (Seinfeld and Pandis, 2006). In this study, the pH of the aqueous layer of Ca(NO$_3$)$_2$ may change dynamically with time during the reaction and may not be completely homogeneous within the aqueous droplet. The pH values could vary between ~ 3 and ~ 7.6. In the surface of the aqueous layer, pH was mainly determined by the gas–aqueous equilibrium of SO$_2$, and was estimated to be ~ 3. In the vicinity of the CaCO$_3$ core, pH was mainly determined by the hydrolysis of carbonate and was estimated to be ~ 7.6. It is likely that both HSO$_3^-$ and SO$_3^{2-}$ were present, and the dominant species depended on the reaction time and location within the aqueous droplet. Nevertheless, to make the reaction mechanism clearer, HSO$_3^-$ was used in the reaction equations. Similar reaction equations are also applicable to SO$_3^{2-}$ because of the fast dissociations of SO$_2 \cdot$H$_2$O and HSO$_3^-$. Overall, the reaction can be written as follows, which clearly shows that O$_2$ was the main oxidant for sulfate formation:

$$2NO_2(aq) + 2HSO_3^-(aq) + (0/1)O_2$$
$$\rightarrow 2NO_2^-(aq) + S_2O_{6/8}^{2-}(aq) + 2H^+(aq) \tag{R19}$$

$$nO_2 + 2nHSO_3^-(aq) \rightarrow 2nSO_4^{2-}(aq) + 2nH^+(aq), \tag{R20}$$

where $n \gg 1$. Once sulfuric acid was formed, it reacted with CaCO$_3$, forming CaSO$_4$:

$$CaCO_3(s) + SO_4^{2-}(aq) + 2H^+(aq) + H_2O(aq)$$
$$\rightarrow CaSO_4 2H_2O(s) + CO_2(g). \tag{R21}$$

As mentioned above, compared with the direct reaction of SO$_2$ with NO$_2$, CaCO$_3$ was consumed more slowly in the reaction with O$_2$ / NO$_2$. There were two possible reasons for

this. First, the $CaSO_4 \cdot 2H_2O$ formed in the reaction could cover the $CaCO_3$ surface and partly suppress the diffusion of aqueous ions, such as protons, and also limit the contact of reactants with the surface of the $CaCO_3$ particles, thus reducing the $CaCO_3$ consumption rate. Second, compared with the direct reaction of SO_2 with NO_2, a much higher fraction of $CaCO_3$ was converted to $CaSO_4 \cdot 2H_2O$ instead of $Ca(NO_3)_2$ due to the fast production of $CaSO_4 \cdot 2H_2O$. Therefore, the volume of a $Ca(NO_3)_2$ droplet was much smaller than that in the direct reaction of SO_2 with NO_2 for a given $CaCO_3$ particle. Because the uptake rate of NO_2 was proportional to the droplet surface area and the NO_2 hydrolysis rate was proportional to the droplet volume, the rate of nitric acid production from NO_2 hydrolysis and its reaction rate with $CaCO_3$ were reduced. Therefore, the $CaCO_3$ particles were consumed more slowly in the reaction with O_2 / NO_2.

4   Conclusion and implications

We investigated the multiphase reaction of SO_2 with $O_2 / NO_2 / H_2O$ on $CaCO_3$ particles. The reaction converted $CaCO_3$ particles to $Ca(NO_3)_2$ droplets, in which $CaSO_4 \cdot 2H_2O$ was embedded and accounted for a significant fraction of the droplet volume by the end of the reaction. The $Ca(NO_3)_2$ droplet formed by the reaction of $CaCO_3$ with NO_2 provided a site for the multiphase oxidation of SO_2. Generally, nitrate and sulfate were formed simultaneously. The reactive uptake coefficient of SO_2 for sulfate formation in the reaction of SO_2 with NO_2 / H_2O in synthetic air was determined to be around 10^{-5}. Compared with the reaction of SO_2 with NO_2 on a $CaCO_3$ particle in the absence of O_2, i.e., the direct oxidation of SO_2 by NO_2 in N_2, the sulfate production rate in the reaction of SO_2 with O_2 / NO_2 was enhanced by 2–3 orders of magnitude. According to the findings of this study and the existing literature, SO_2 oxidation likely proceeded via a free-radical chain reaction mechanism. O_2 was the main oxidant of SO_2, and NO_2 mainly acted as an initiator of the chain reactions. The synergy of NO_2 and O_2 resulted in the fast oxidation of SO_2. The absence of either NO_2 or O_2 led to much slower SO_2 oxidation.

Using a method developed in our previous study (Zhao et al., 2018), we assessed the importance of the multiphase oxidation of SO_2 by O_2 in the presence of NO_2 by estimating the lifetime of SO_2 due to multiphase reactions and the lifetime due to the gas-phase reaction (with the OH radical). The lifetime of SO_2 due to the multiphase reaction of SO_2 with O_2 / NO_2 was estimated to be around 20 days using the reactive uptake coefficient of SO_2 (1.2×10^{-5}) and the typical particle surface area concentration for mineral aerosols in winter in Beijing (6.3×10^{-6} $cm^2 cm^{-3}$) (Huang et al., 2015). This lifetime is comparable to the lifetime of SO_2 due to the gas-phase reaction with OH, which is ~ 12 days, assuming that the daytime OH concentration is 1×10^6 molecules cm^{-3} (Lelieveld et al., 2016; Prinn et al.,

2005). Therefore, we conclude that the multiphase oxidation of SO_2 by O_2 in the presence of NO_2 is likely to be an important source of sulfate and a sink of SO_2 in the ambient atmosphere, and can play a significant role in the sulfate formation during severe haze episodes, such as those that frequently occur in China. During haze episodes, there are high concentrations of SO_2 and NO_2 and relative humidity is often high (Zhang et al., 2014; Zheng et al., 2015b; Wang et al., 2016). Under these conditions, the multiphase oxidation of SO_2 by O_2 in the presence of NO_2 could proceed rapidly, forming sulfate. The enhanced sulfate concentration due to multiphase reactions and resulting aerosol water content can further promote the multiphase oxidation of SO_2. The reaction thus proceeds in a self-accelerating way. Therefore, it can contribute significantly to sulfate formation during haze episodes, which could explain the discrepancies between the observed and modeled sulfate concentrations (Cheng et al., 2016; Gao et al., 2016; Wang et al., 2016; Zheng et al., 2015a).

In addition, elucidating the mechanism of the multiphase reaction of SO_2 with $O_2 / NO_2 / H_2O$ in the atmosphere is important for the other atmospheric implications of the reaction besides sulfate formation. According to the reaction mechanism, the direct oxidation of SO_2 by NO_2 forms sulfate and nitrite, with a stoichiometry of $1 : 1$, and nitrite can further form HONO under acidic conditions. The HONO could then evaporate into the atmosphere, where it would be an important source of OH radicals. If NO_2 were the main oxidant of SO_2 in the multiphase reaction, the reaction would form one HONO molecule for every sulfate molecule formed. Thus, the oxidation of SO_2 by NO_2 can simultaneously be an important source of HONO and OH radicals, and SO_2 oxidation would be strongly coupled with reactive nitrogen chemistry. However, according to the mechanism of this study, NO_2 only acted as an initiator of the chain reactions in SO_2 oxidation and essentially all the SO_2 was oxidized by O_2. Therefore, the amount of HONO formation per sulfate molecule formed was trivial. The oxidation of SO_2 by O_2 / NO_2 is expected to be neither an important source of HONO and OH in the atmosphere nor to have a significant influence on reactive nitrogen chemistry.

In this study, we investigated the reaction of SO_2 with O_2 in the presence of NO_2 at three O_2 concentrations. The influence of the O_2 concentration was shown to be significant. Future experimental results with more O_2 concentration levels would provide more insight into the reaction mechanism and process.

In addition, in the ambient atmosphere, the internal mixing of organics with S(IV) in particles may influence the S(IV) oxidation rate by O_2 in the presence of NO_2. When organics are abundant in particles, for example during haze episodes in China, they can react with and thus scavenge radical anion carriers such as $SO_5^{\bullet-}$ and $SO_4^{\bullet-}$ (Herrmann, 2003; Herrmann et al., 2015; Huie, 1995). Therefore, the presence of internally mixed organics can reduce the effectivity of the po-

tential radical reaction chain and of S(IV) oxidation, which can undermine the importance of the oxidation by O$_2$ in the presence of NO$_2$ in the overall S(IV) oxidation.

References

Brandt, C. and Vaneldik, R.: Transition metal-catalyzed oxidation of sulfur (IV) oxides. Atmospheric-relevant processes and mechanisms, Chem. Rev., 95, 119–190, https://doi.org/10.1021/cr00033a006, 1995.

Brandt, C., Fabian, I., and Vaneldik, R.: Kinetics and mechanism of the iron(III)-catalyzed autoxidation of sulfur(IV) oxides in aqueous-solution – evidence for the redox cycling of iron in the presence of oxygen and modeling of the overall reaction-mechanism, Inorg. Chem., 33, 687–701, https://doi.org/10.1021/ic00082a012, 1994.

Chameides, W. L. and Davis, D. D.: The free-radical chemistry of cloud droplets and its impact upon the composition of rain, J. Geophys. Res.-Oceans, 87, 4863–4877, https://doi.org/10.1029/JC087iC07p04863, 1982.

Cheng, Y. F., Zheng, G. J., Wei, C., Mu, Q., Zheng, B., Wang, Z. B., Gao, M., Zhang, Q., He, K. B., Carmichael, G., Poschl, U., and Su, H.: Reactive nitrogen chemistry in aerosol water as a source of sulfate during haze events in China, Sci. Adv., 2, e1601530, https://doi.org/10.1126/sciadv.1601530, 2016.

Clifton, C. L., Altstein, N., and Huie, R. E.: Rate-constant for the reaction of NO$_2$ with sulfur(IV) over the pH range 5.3–13, Environ. Sci. Technol., 22, 586–589, https://doi.org/10.1021/es00170a018, 1988.

Davidovits, P., Kolb, C. E., Williams, L. R., Jayne, J. T., and Worsnop, D. R.: Mass accommodation and chemical reactions at gas-liquid interfaces, Chem. Rev., 106, 1323–1354, https://doi.org/10.1021/cr040366k, 2006.

Deister, U. and Warneck, P.: Photooxidation of sulfite (SO_3^{2-}) in aqueous solution, J. Phys. Chem., 94, 2191–2198, https://doi.org/10.1021/j100368a084, 1990.

Eriksen, T. E.: pH Effects on the pulse radiolysis of de-oxygenated aqueous solutions of sulphur dioxide, Jour-nal of the Chemical Society, Faraday Transactions 1: Physical Chemistry in Condensed Phases, 70, 208–215, https://doi.org/10.1039/f19747000208, 1974.

Gao, M., Carmichael, G. R., Wang, Y., Ji, D., Liu, Z., and Wang, Z.: Improving simulations of sulfate aerosols during winter haze over Northern China: the impacts of heterogeneous oxidation by NO$_2$, Front. Environ. Sci. En., 10, 16, https://doi.org/10.1007/s11783-016-0878-2, 2016.

Guo, H., Weber, R. J., and Nenes, A.: High levels of ammonia do not raise fine particle pH sufficiently to yield nitrogen oxide-dominated sulfate production, Sci. Rep., 7, 12109, https://doi.org/10.1038/s41598-017-11704-0, 2017.

Hayon, E., Treinin, A., and Wilf, J.: Electronic spectra, photochemistry, and autoxidation mechanism of the sulfite-bisulfite-pyrosulfite systems. SO$_2$-, SO$_3$-, SO$_4$-, and SO$_5$-radicals, J. Am. Chem. Soc. , 94, 47–57, https://doi.org/10.1021/ja00756a009, 1972.

He, H., Wang, Y., Ma, Q., Ma, J., Chu, B., Ji, D., Tang, G., Liu, C., Zhang, H., and Hao, J.: Mineral dust and NO$_x$ promote the conversion of SO$_2$ to sulfate in heavy pollution days, Sci. Rep., 4, 4172, https://doi.org/10.1038/srep04172, 2014.

Herrmann, H.: Kinetics of aqueous phase reactions relevant for atmospheric chemistry, Chem. Rev., 103, 4691–4716, https://doi.org/10.1021/cr020658q, 2003.

Herrmann, H., Schaefer, T., Tilgner, A., Styler, S. A., Weller, C., Teich, M., and Otto, T.: Tropospheric Aqueous-Phase Chemistry: Kinetics, Mechanisms, and Its Coupling to a Changing Gas Phase, Chem. Rev., 115, 4259–4334, https://doi.org/10.1021/cr500447k, 2015.

Huang, L., Zhao, Y., Li, H., and Chen, Z.: Kinetics of Heterogeneous Reaction of Sulfur Dioxide on Authentic Mineral Dust: Effects of Relative Humidity and Hydrogen Peroxide, Environ. Sci. Technol., 49, 10797–10805, https://doi.org/10.1021/acs.est.5b03930, 2015.

Huie, R. E. and Neta, P.: Kinetics of one-electron transfer-reactions involving ClO$_2$ and NO$_2$, J. Phys. Chem. , 90, 1193–1198, https://doi.org/10.1021/j100278a046, 1986.

Huie, R. E. and Neta, P.: Rate constants for some oxidations of S(IV) by radicals in aqueous-solutions, Atmos. Environ., 21, 1743–1747, https://doi.org/10.1016/0004-6981(87)90113-2, 1987.

Huie, R. E., Clifton, C. L., and Altstein, N.: A pulse radiolysis and flash photolysis study of the radicals SO$_2$, SO$_3$, SO$_4$ and SO$_5$, Radiat. Phys. Chem., 33, 361–370, 1989.

Huie, R. E.: Free radical chemistry of the atmospheric aqueous phase, in: Progress and Problems in Atmospheric Chemistry, WORLD SCIENTIFIC, Singapore, 374–419, 1995.

Lee, Y.-N. and Schwartz, S. E.: Kinetics of oxidation of aqueous sulfur (IV) by nitrogen dioxide, in: Precipitation Scavenging, Dry Deposition and Resuspension, edited by: Pruppacher, H. R., Semonin, R. G., and Slinn, W. G. N., Elsevier, New York, 453–466, 1983.

Lelieveld, J., Gromov, S., Pozzer, A., and Taraborrelli, D.: Global tropospheric hydroxyl distribution, budget and reactivity, Atmos. Chem. Phys., 16, 12477–12493, https://doi.org/10.5194/acp-16-12477-2016, 2016.

Li, H. J., Zhu, T., Zhao, D. F., Zhang, Z. F., and Chen, Z. M.: Kinetics and mechanisms of heterogeneous reaction of NO$_2$ on CaCO$_3$ surfaces under dry and wet conditions, Atmos. Chem.

Phys., 10, 463–474, https://doi.org/10.5194/acp-10-463-2010, 2010.

Littlejohn, D., Wang, Y. Z., and Chang, S. G.: Oxidation of aqueous sulfite ion by nitrogen-dioxide, Environ. Sci. Technol., 27, 2162–2167, https://doi.org/10.1021/es00047a024, 1993.

Liu, M. X., Song, Y., Zhou, T., Xu, Z. Y., Yan, C. Q., Zheng, M., Wu, Z. J., Hu, M., Wu, Y. S., and Zhu, T.: Fine particle pH during severe haze episodes in northern China, Geophys. Res. Lett., 44, 5213–5221, https://doi.org/10.1002/2017gl073210, 2017.

Liu, Y. J., Zhu, T., Zhao, D. F., and Zhang, Z. F.: Investigation of the hygroscopic properties of Ca(NO$_3$)$_2$ and internally mixed Ca(NO$_3$)$_2$ / CaCO$_3$ particles by micro-Raman spectrometry, Atmos. Chem. Phys., 8, 7205–7215, https://doi.org/10.5194/acp-8-7205-2008, 2008.

Ma, Q., He, H., Liu, Y., Liu, C., and Grassian, V. H.: Heterogeneous and multiphase formation pathways of gypsum in the atmosphere, Phys. Chem. Chem. Phys., 15, 19196-19204, 10.1039/c3cp53424c, 2013.

Nakamoto, K.: Infrared and Raman Spectra of Inorganic and Coordination Compounds Part A, John Wiley &Sons, New York, 221–247, 1997.

Nash, T.: Effect of nitrogen-dioxide and of some transition-metals on the oxidation of dilute bisulfite solutions, Atmos. Environ., 13, 1149–1154, https://doi.org/10.1016/0004-6981(79)90038-6, 1979.

Podkrajšek, B., Grgić, I., and Turšič, J.: Determination of sulfur oxides formed during the S(IV) oxidation in the presence of iron, Chemosphere, 49, 271–277, https://doi.org/10.1016/S0045-6535(02)00324-7, 2002.

Pöschl, U., Rudich, Y., and Ammann, M.: Kinetic model framework for aerosol and cloud surface chemistry and gas-particle interactions – Part 1: General equations, parameters, and terminology, Atmos. Chem. Phys., 7, 5989–6023, https://doi.org/10.5194/acp-7-5989-2007, 2007.

Prinn, R. G., Huang, J., Weiss, R. F., Cunnold, D. M., Fraser, P. J., Simmonds, P. G., McCulloch, A., Harth, C., Reimann, S., Salameh, P., O'Doherty, S., Wang, R. H. J., Porter, L. W., Miller, B. R., and Krummel, P. B.: Evidence for variability of atmospheric hydroxyl radicals over the past quarter century, Geophys. Res. Lett., 32, L07809, https://doi.org/10.1029/2004gl022228, 2005.

Santachiara, G., Prodi, F., and Vivarelli, F.: SO$_2$ oxidation in monodisperse droplets grown on carbon nuclei in presence of NO$_2$, J. Aerosol Sci., 21, S221–S224, https://doi.org/10.1016/0021-8502(90)90224-l, 1990.

Santachiara, G., Prodi, F., and Vivarelli, F.: Further experiments on SO$_2$ oxidation rate in monodisperse droplets grown on carbon nuclei in presence of O-2 and NO$_2$, J. Aerosol Sci., 24, 683–685, https://doi.org/10.1016/0021-8502(93)90024-4, 1993.

Sarma, L. P., Prasad, P. S. R., and Ravikumar, N.: Raman spectroscopic study of phase transitions in natural gypsum, J. Raman Spectrosc., 29, 851–856, https://doi.org/10.1002/(sici)1097-4555(199809)29:9<851::aid-jrs313>3.0.co;2-s, 1998.

Seinfeld, J. H. and Pandis, S. N.: Atmospheric chemistry and physics: from air pollution to climate change, 2nd Edn., John Wiley &Sons. Inc., 2006.

Shen, C. H. and Rochelle, G. T.: Nitrogen Dioxide Absorption and Sulfite Oxidation in Aqueous Sulfite, Environ. Sci. Technol., 32, 1994–2003, https://doi.org/10.1021/es970466q, 1998.

Shi, X. L.: Generation of SO$_3^-$ and OH radicals in SO$_3^{2-}$ reactions with inorganic environmental-pollutants and its implications to SO$_3^{2-}$ toxicity, J. Inorg. Biochem., 56, 155–165, https://doi.org/10.1016/0162-0134(94)85002-x, 1994.

Spindler, G., Hesper, J., Bruggemann, E., Dubois, R., Muller, T., and Herrmann, H.: Wet annular denuder measurements of nitrous acid: laboratory study of the artefact reaction of NO$_2$ with S(IV) in aqueous solution and comparison with field measurements, Atmos. Environ., 37, 2643–2662, https://doi.org/10.1016/s1352-2310(03)00209-7, 2003.

Turšič, J., Grgić, I., and Bizjak, M.: Influence of NO$_2$ and dissolved iron on the S(IV) oxidation in synthetic aqueous solution, Atmos. Environ., 35, 97–104, https://doi.org/10.1016/S1352-2310(00)00283-1, 2001.

Wang, G., Zhang, R., Gomez, M. E., Yang, L., Levy Zamora, M., Hu, M., Lin, Y., Peng, J., Guo, S., Meng, J., Li, J., Cheng, C., Hu, T., Ren, Y., Wang, Y., Gao, J., Cao, J., An, Z., Zhou, W., Li, G., Wang, J., Tian, P., Marrero-Ortiz, W., Secrest, J., Du, Z., Zheng, J., Shang, D., Zeng, L., Shao, M., Wang, W., Huang, Y., Wang, Y., Zhu, Y., Li, Y., Hu, J., Pan, B., Cai, L., Cheng, Y., Ji, Y., Zhang, F., Rosenfeld, D., Liss, P. S., Duce, R. A., Kolb, C. E., and Molina, M. J.: Persistent sulfate formation from London Fog to Chinese haze, P. Natl. Acad. Sci. USA, 113, 13630–13635, https://doi.org/10.1073/pnas.1616540113, 2016.

Waygood, S. J. and McElroy, W. J.: Spectroscopy and decay kinetics of the sulfite radical anion in aqueous solution, J. Chem. Soc.-Faraday Trans., 88, 1525–1530, https://doi.org/10.1039/ft9928801525, 1992.

Xue, J., Yuan, Z. B., Griffith, S. M., Yu, X., Lau, A. K. H., and Yu, J. Z.: Sulfate Formation Enhanced by a Cocktail of High NO$_x$, SO$_2$, Particulate Matter, and Droplet pH during Haze-Fog Events in Megacities in China: An Observation-Based Modeling Investigation, Environ. Sci. Technol., 50, 7325–7334, https://doi.org/10.1021/acs.est.6b00768, 2016.

Zhang, J. K., Sun, Y., Liu, Z. R., Ji, D. S., Hu, B., Liu, Q., and Wang, Y. S.: Characterization of submicron aerosols during a month of serious pollution in Beijing, 2013, Atmos. Chem. Phys., 14, 2887–2903, https://doi.org/10.5194/acp-14-2887-2014, 2014.

Zhao, D., Song, X., Zhu, T., Zhang, Z., Liu, Y., and Shang, J.: Multiphase oxidation of SO$_2$ by NO$_2$ on CaCO$_3$ particles, Atmos. Chem. Phys., 18, 2481–2493, https://doi.org/10.5194/acp-18-2481-2018, 2018.

Zhao, D. F., Zhu, T., Chen, Q., Liu, Y. J., and Zhang, Z. F.: Raman micro-spectrometry as a technique for investigating heterogeneous reactions on individual atmospheric particles, Sci. China Chem., 54, 154–160, https://doi.org/10.1007/s11426-010-4182-x, 2011.

Zheng, B., Zhang, Q., Zhang, Y., He, K. B., Wang, K., Zheng, G. J., Duan, F. K., Ma, Y. L., and Kimoto, T.: Heterogeneous chemistry: a mechanism missing in current models to explain secondary inorganic aerosol formation during the January 2013 haze episode in North China, Atmos. Chem. Phys., 15, 2031–2049, https://doi.org/10.5194/acp-15-2031-2015, 2015a.

Zheng, G. J., Duan, F. K., Su, H., Ma, Y. L., Cheng, Y., Zheng, B., Zhang, Q., Huang, T., Kimoto, T., Chang, D., Pöschl, U., Cheng, Y. F., and He, K. B.: Exploring the severe winter haze in Beijing: the impact of synoptic weather, regional transport and heterogeneous reactions, Atmos. Chem. Phys., 15, 2969–2983, https://doi.org/10.5194/acp-15-2969-2015, 2015b.

Zhu, T., Shang, J., and Zhao, D. F.: The roles of heterogeneous chemical processes in the formation of an air pollution complex and gray haze, Sci. China Chem., 54, 145–153, https://doi.org/10.1007/s11426-010-4181-y, 2011.